European Journal of Mechanics A/Solids 28 (2009) 248–256

Contents lists available at ScienceDirect

European Journal of Mechanics A/Solids

www.elsevier.com/locate/ejmsol

Non-linear analysis of functionally graded plates in cylindrical bending under thermomechanical loadings based on a layerwise theory

Masoud Tahani [a,*], Seyed Mahdi Mirzababaee [a,b]

[a] Department of Mechanical Engineering, Faculty of Engineering, Ferdowsi University of Mashhad, Mashhad, Iran
[b] Khorasan Research Center for Technology Development (KRCTD), Quchan Highway, Mashhad, Iran

ARTICLE INFO

Article history:
Received 8 September 2007
Accepted 16 May 2008
Available online 4 June 2008

Keywords:
Functionally graded material
Geometric non-linearity
Plate
Analytical solution
Layerwise method

ABSTRACT

A layerwise theory is used to analyze analytically displacements and stresses in functionally graded composite plates in cylindrical bending subjected to thermomechanical loadings. The plates are assumed to have isotropic, two-constituent material distribution through the thickness, and the modulus of elasticity of the plate is assumed to vary according to a power-law distribution in terms of the volume fractions of the constituents. The non-linear strain–displacement relations in the von Kármán sense are used to study the effect of geometric non-linearity. The equilibrium equations are solved exactly and also by using a perturbation technique. Numerical results are presented to show the effect of the material distribution on the deflections and stresses.

1. Introduction

In conventional laminated composite materials, there is a high chance that debonding will occur at some extreme loading conditions. On the other hand, gradually varying the volume fraction of the constituents can resolve this problem. Functionally graded materials (FGMs) are composite materials which exhibit a progressive change in composition, structure, and properties as a function of spatial direction within the material.

Many studies for thermal stress and linear thermal bending of FGM plates are available in the literature (e.g., see Noda and Tsuji, 1991; Tanigawa et al., 1996; Reddy and Chin, 1998). However, investigations in non-linear analysis of FGM plates under thermal or mechanical loading are limited in number. For example, Praveen and Reddy (1998) investigated the response of functionally graded (FG) ceramic-metal plates using a plate finite element that accounts for the transverse shear strains, rotary inertia and moderately large rotations in the von Kármán sense. Reddy (2000) presented solutions for rectangular functionally graded plates based on the third-order shear deformation plate theory. The formulation accounted for the thermomechanical coupling, time dependency, and the von Kármán-type geometric non-linearity. Using an asymptotic method, the three-dimensional thermomechanical deformations of functionally graded rectangular plate were investigated by Reddy and Cheng (2001) and the distributions of temperature, displacements and stresses in the plate were calculated for different volume fraction of ceramic constituent.

Shen (2002) analyzed non-linear bending of a simply supported, functionally graded rectangular plate subjected to a transverse uniform or sinusoidal load and in thermal environments. The governing equations were obtained based on Reddy's higher-order shear deformation plate theory and these equations were solved by a mixed Galerkin-perturbation technique. Based on the von Kármán theory, Woo and Meguid (2001) derived an analytical solution expressed in terms of Fourier series for the large deflection of functionally graded plates and shallow shells under transverse mechanical loading and a temperature field. Yang and Shen (2003) using a semi-analytical approach analyzed the non-linear bending and post-buckling behaviors of FG rectangular plates subjected to combined action of transverse and in-plane loads. Tahani et al. (2006) analytically analyzed functionally graded beams subjected to thermomechanical loadings based on a first-order shear deformation theory. Hsieh and Lee (2006) solved the inverse problem of a functionally graded elliptical plate with large deflection and disturbed boundary under uniform load. They derived the governing equations of a thin plate with large deflection based on the classical non-linear von Kármán plate theory. Then they employed a perturbation technique on displacement terms in conjunction with Taylor series expansion of the disturbed boundary conditions to solve the non-classical problem. Agarwal et al. (2006) used the existing statically exact beam finite element based on the first order shear deformation theory to study the geometric non-linear effects on static and dynamic responses in isotropic, composite and functionally graded material beams. They utilized both von Kármán strain tensor and Green's strain tensor in the static case, whereas,

* Corresponding author. Tel.: +98 511 876 3304; fax: +98 511 882 9541.
E-mail address: mtahani@ferdowsi.um.ac.ir (M. Tahani).

0997-7538/$ – see front matter
doi:10.1016/j.euromechsol.2008.05.002

for the wave propagation studies only the von Kármán strains were used.

It is intended here to accurately determine the displacements and stresses in functionally graded plates in cylindrical bending subjected to thermomechanical loadings. To this end, based on a layerwise theory the governing equations are obtained. The nonlinear strain–displacement relations are used to study the effect of geometric non-linearity. The equilibrium equations are solved exactly for FGM plates with the identical boundary conditions and also by using a perturbation technique for FGM plates with general boundary conditions. Numerical results are presented to show the influence of material properties, plate geometry, mechanical loading and the temperature field on the resulting transverse deflection and stress state.

2. Theoretical formulation

2.1. Displacement field and strains

Consider a functionally graded plate of thickness h, side length a in the x-direction, and infinite extent in the y-direction. Since the plate is long in the y-direction, it may be assumed that a state of plane strain exists. Hence, the following displacement field is assumed:

$$\begin{aligned} &u_1(x,y,z) = u_0(x) + U_k(x)\Phi_k(z), \quad k = 1,2,\ldots,N+1,\\ &u_2(x,y,z) = 0,\\ &u_3(x,y,z) = w(x). \end{aligned} \tag{1}$$

It is to be noted that a repeated index indicates summation over all values of that index. In Eqs. (1) u_1, u_2, and u_3 represent the displacement components in the x, y, and z directions, respectively, of a material point initially located at (x, y, z) in the undeformed laminate. Also u_0 and w are the displacement components of all points in the middle surface of the plate in the x- and z-directions, respectively, U_k $(k = 1, 2, \ldots, N+1)$ is the displacement component of all points located on the kth plane in the x-direction, and Φ_k is a continuous function of the thickness coordinate z (global interpolation function). Also N denotes the total number of numerical layers considered in a plate.

It is noted that in the layerwise theory the accuracy of the displacement field in Eqs. (1) depends on the shape function $\Phi_k(z)$ and the number of surfaces in the plate. Here, $\Phi_k(z)$ is assumed to be a linear interpolation function. On the other hand, the number of surfaces may be increased by subdividing total thickness of the plate into a number of numerical layers. The local Lagrangian linear interpolation functions within, say, the kth numerical layer are defined as follows:

$$\phi_k^1 = \frac{z_{k+1} - z}{h_k}, \qquad \phi_k^2 = \frac{z - z_k}{h_k} \tag{2}$$

where h_k is the thickness of the kth numerical layer and z_k denotes the z-coordinate of the bottom of the kth numerical layer. This way, the global interpolation function $\Phi_k(z)$ may be presented as (see Reddy, 1987; Nosier et al., 1993; Tahani and Nosier, 2003):

$$\Phi_k(z) = \begin{cases} 0, & z \leqslant z_{k-1},\\ \phi_{k-1}^2(z), & z_{k-1} \leqslant z \leqslant z_k,\\ \phi_k^1(z), & z_k \leqslant z \leqslant z_{k+1},\\ 0, & z \geqslant z_{k+1}, \end{cases} \quad k = 1,2,\ldots,N+1. \tag{3}$$

In the present study we wish to investigate the effect of geometric non-linearity on the response quantities. Therefore, the von Kármán-type of geometric non-linearity is taken into consideration in the strain–displacement relations. Substituting Eqs. (1) in the appropriate strain–displacement relations (Fung, 1965) results in:

$$\begin{aligned} &\varepsilon_x = \frac{du_0}{dx} + \frac{1}{2}\left(\frac{dw}{dx}\right)^2 + \frac{dU_k}{dx}\Phi_k, \qquad \varepsilon_y = \varepsilon_z = 0,\\ &\gamma_{xy} = \gamma_{yz} = 0, \qquad \gamma_{xz} = \frac{dw}{dx} + U_k\frac{d\Phi_k}{dz}. \end{aligned} \tag{4}$$

2.2. Constitutive relations

Consider a functionally graded plate, which is made from a mixture of ceramics and metals. It is assumed that the composition properties of FGM vary through the thickness of the plate. The variation of material properties can be expressed as:

$$p(z) = (p_t - p_b)V_t + p_b, \tag{5}$$

where p denotes a generic material property like modulus and p_t and p_b denote the corresponding properties of the top and bottom faces of the plate, respectively. Also V_t in Eq. (5) denotes the volume fraction of the top face constituent and follows a simple power-law as:

$$V_t = \left(\frac{z}{h} + \frac{1}{2}\right)^n, \tag{6}$$

where h is the total thickness of the plate, z is the thickness coordinate $(-h/2 \leqslant z \leqslant h/2)$, and n $(0 \leqslant n \leqslant \infty)$ is a parameter that dictates the material variation profile through the thickness. Here we assume that moduli E and G, coefficient of thermal expansion α, and thermal conductivity k vary according to Eq. (5) and the Poisson's ratio ν is assumed to be a constant.

The linear constitutive relations are:

$$\begin{aligned} &\begin{Bmatrix} \sigma_x\\ \sigma_y\\ \sigma_{xy} \end{Bmatrix} = \begin{bmatrix} Q_{11} & Q_{12} & 0\\ Q_{12} & Q_{22} & 0\\ 0 & 0 & Q_{66} \end{bmatrix}\left(\begin{Bmatrix} \varepsilon_x\\ \varepsilon_y\\ \gamma_{xy} \end{Bmatrix} - \begin{pmatrix} 1\\ 1\\ 0 \end{pmatrix}\alpha\Delta T\right),\\ &\begin{Bmatrix} \sigma_{yz}\\ \sigma_{xz} \end{Bmatrix} = \begin{bmatrix} Q_{44} & 0\\ 0 & Q_{55} \end{bmatrix}\begin{Bmatrix} \gamma_{yz}\\ \gamma_{xz} \end{Bmatrix}, \end{aligned} \tag{7}$$

where

$$\begin{aligned} &Q_{11} = Q_{22} = \frac{E(z)}{1-\nu^2}, \qquad Q_{12} = \frac{\nu E(z)}{1-\nu^2},\\ &Q_{44} = Q_{55} = Q_{66} = \frac{E(z)}{2(1+\nu)} = G(z), \end{aligned} \tag{8}$$

and ΔT is the temperature change from a stress-free state that will be obtained by solving the one-dimensional heat transfer equation.

2.3. Equilibrium equations

Using the principle of virtual displacements (Fung, 1965), the equilibrium equations can be shown to be (see Reddy, 1987):

$$\delta u_0: \quad \frac{dN_x}{dx} = 0, \tag{9a}$$

$$\delta U_k: \quad \frac{dM_x^k}{dx} - Q_x^k = 0, \quad k = 1,2,\ldots,N+1, \tag{9b}$$

$$\delta w: \quad \frac{dQ_x}{dx} + \frac{d}{dx}\left(N_x\frac{dw}{dx}\right) + q(x) = 0, \tag{9c}$$

where $q(x)$ is the transverse load on the top surface of the plate. In Eqs. (9) the generalized stress resultants are defined as:

$$\begin{aligned} &(N_x, Q_x) = \int_{-h/2}^{h/2} (\sigma_x, \sigma_{xz})\,dz,\\ &\left(M_x^k, Q_x^k\right) = \int_{-h/2}^{h/2} \left(\sigma_x\Phi_k, \sigma_{xz}\frac{d\Phi_k}{dz}\right)dz. \end{aligned} \tag{10}$$

The boundary conditions consist of specifying the following quantities at $x = \pm a/2$:

Geometric (Essential)	Force (Natural)
u_0	N_x
U_k	M_x^k
w	$N_x\frac{dw}{dx} + Q_x$

(11)

Upon substitution of Eqs. (4) into Eqs. (7) and the subsequent results into Eqs. (10), the generalized stress resultants in terms of displacement components will be obtained which can be presented as follows:

$$N_x = A_{11}\left[\frac{du_0}{dx} + \frac{1}{2}\left(\frac{dw}{dx}\right)^2\right] + B_{11}^j\frac{dU_j}{dx} - N_x^T,$$
$$M_x^k = B_{11}^k\left[\frac{du_0}{dx} + \frac{1}{2}\left(\frac{dw}{dx}\right)^2\right] + D_{11}^{kj}\frac{dU_j}{dx} - M_x^{k(T)},$$
$$Q_x = A_{55}\frac{dw}{dx} + A_{55}^j U_j, \qquad Q_x^k = A_{55}^k\frac{dw}{dx} + A_{55}^{kj}U_j, \tag{12}$$

where

$$A_{jl} = \sum_{i=1}^{N}\int_{z_i}^{z_{i+1}} Q_{jl}^{(i)}\,dz, \quad jl = 11, 55,$$
$$A_{55}^k = \sum_{i=1}^{N}\int_{z_i}^{z_{i+1}} Q_{55}^{(i)}\frac{d\Phi_k}{dz}\,dz, \qquad B_{11}^k = \sum_{i=1}^{N}\int_{z_i}^{z_{i+1}} Q_{11}^{(i)}\Phi_k\,dz,$$
$$A_{55}^{kj} = \sum_{i=1}^{N}\int_{z_i}^{z_{i+1}} Q_{55}^{(i)}\frac{d\Phi_k}{dz}\frac{d\Phi_j}{dz}\,dz, \qquad D_{11}^{kj} = \sum_{i=1}^{N}\int_{z_i}^{z_{i+1}} Q_{11}^{(i)}\Phi_k\Phi_j\,dz. \tag{13}$$

The thermal resultants in Eqs. (12) are defined as:

$$\left(N_x^T, M_x^{k(T)}\right) = \sum_{i=1}^{N}\int_{z_i}^{z_{i+1}}\left(Q_{11}^{(i)} + Q_{12}^{(i)}\right)(1, \Phi_k)\alpha\,\Delta T\,dz. \tag{14}$$

Lastly, the governing equations of equilibrium are obtained by substituting Eqs. (12) into Eqs. (9).

3. Analytical solutions

In this study it is assumed that a functionally graded plate is subjected to a uniform transverse load on its top surface and/or a thermal load. It is intended here to obtain analytical solutions for the non-linear bending of the FGM plate by using two methods, exact and perturbation technique. In the first method the solution can only be obtained for plates with symmetric loading and boundary conditions. But in the latter method the solution can be obtained for symmetric and unsymmetric plates.

In order to solve the equilibrium equations in thermal loadings the temperature field should be known. It is assumed that one value of temperature is imposed on the bottom surface and the other value on the top surface of the plate. In this case, the temperature distribution through the thickness can be obtained by solving a simple steady state heat transfer equation through the thickness of the plate. This equation is given by:

$$-\frac{d}{dz}\left(k(z)\frac{dT}{dz}\right) = 0, \tag{15}$$

with the boundary conditions $T = T_b$ at $z = -h/2$ and $T = T_t$ at $z = h/2$. Integration of Eq. (15) gives us:

$$dT = \frac{c_1\,dz}{k(z)} = \frac{c_1\,dz}{(k_t - k_b)(\frac{z}{h} + \frac{1}{2})^n + k_b}, \tag{16}$$

where c_1 being a constant of integration. Now by choosing $\xi = \frac{z}{h} + \frac{1}{2}$, Eq. (16) can be shown to be:

$$dT = \frac{c_1 h\,d\xi}{(k_t - k_b)(\xi^n - \mu^n)}, \tag{17}$$

where $\mu^n = -k_b/(k_t - k_b)$. It is readily seen that the solution to Eq. (17) is:

$$T = \frac{c_1 h A(\xi)}{k_t - k_b} + c_2, \tag{18}$$

where $A(\xi) = \int \frac{d\xi}{\xi^n - \mu^n}$. The constants of integration c_1 and c_2 in Eq. (18) are found by imposing the thermal boundary conditions at the top and bottom surfaces of the plate as follows:

$$c_1 = \frac{(T_t - T_b)(k_t - k_b)}{h[A(1) - A(0)]}, \qquad c_2 = -\frac{T_b A(1) - T_t A(0)}{A(1) - A(0)}. \tag{19}$$

It is to be noted that the integral of $A(\xi)$ has analytical solution for $n = 0.2$, $n = 0.5$, and all integer values. For other values of n, this integral must be solved numerically.

In what follows two solution methodologies for Eqs. (9) are presented.

3.1. Exact solutions

In this section, it is assumed that the plate is subjected to a symmetric transverse load and the boundary conditions of the plate at $x = \pm a/2$ are identical. Before discussing the procedure adopted for solving Eqs. (9), it is appropriate to indicate here that in the present layerwise theory two types of simple supports at the edges of the plate (i.e., at $x = \pm a/2$) may be classified, namely:

$$\text{S1:} \quad u_0 = M_x^k = w = 0, \tag{20a}$$
$$\text{S3:} \quad N_x = M_x^k = w = 0. \tag{20b}$$

Also two types of clamped supports may be classified, namely:

$$\text{C1:} \quad u_0 = U_k = w = 0, \tag{21a}$$
$$\text{C3:} \quad N_x = U_k = w = 0. \tag{21b}$$

It is to be noted that these types of boundary conditions are defined similar to the definitions in the equivalent single-layer theories. For simplicity, the boundary conditions of a composite plate in cylindrical bending may be represented in a concise rule. For example, a plate with the edge conditions C1 at $x = -a/2$ and S3 at $x = a/2$ may be called C1–S3.

In order to obtain the exact solutions of equilibrium equations (9), Eq. (9a) is integrated with respect to x to yield:

$$N_x = N_x^0 \quad \text{or} \quad A_{11}\left[\frac{du_0}{dx} + \frac{1}{2}\left(\frac{dw}{dx}\right)^2\right] + B_{11}^j\frac{dU_j}{dx} = N_x^0 + N_x^T, \tag{22}$$

where N_x^0 is a constant of integration. Next from Eq. (22), the following expression is obtained:

$$\frac{du_0}{dx} + \frac{1}{2}\left(\frac{dw}{dx}\right)^2 = \frac{1}{A_{11}}\left(N_x^0 + N_x^T - B_{11}^j\frac{dU_j}{dx}\right). \tag{23}$$

Substituting Eq. (23) into Eqs. (12) and the subsequent results into Eqs. (9b) and (9c) to yield:

$$\left(D_{11}^{kj} - \frac{B_{11}^k B_{11}^j}{A_{11}}\right)\frac{d^2U_j}{dx^2} - A_{55}^{kj}U_j - A_{55}^k\frac{dw}{dx} = 0, \tag{24a}$$
$$A_{55}^j\frac{dU_j}{dx} + \left(A_{55} + N_x^0\right)\frac{d^2w}{dx^2} = -q(x). \tag{24b}$$

Eqs. (24) are $N + 2$ linear ordinary differential equations with constant coefficients. It is to be noted that there exist repeated

zero roots (or eigenvalues) in the characteristic equation of the set of equations in (24). In order to enhance the solution scheme of these equations, some small artificial terms will be added to these equations so that the characteristic roots become all distinct (see Tahani and Nosier, 2004):

$$\left(D_{11}^{kj}-\frac{B_{11}^{k}B_{11}^{j}}{A_{11}}\right)\frac{d^2U_j}{dx^2}-A_{55}^{kj}U_j-A_{55}^{k}\frac{dw}{dx}=\varepsilon^{kj}U_j, \tag{25a}$$

$$A_{55}^{j}\frac{dU_j}{dx}+\left(A_{55}+N_x^0\right)\frac{d^2w}{dx^2}=-q(x)+\varepsilon w, \tag{25b}$$

where

$$\varepsilon^{kj}=\varepsilon\int_{-h/2}^{h/2}\Phi_k\Phi_j\,dz, \tag{26}$$

with ε being a prescribed small number.

Next, Eqs. (25) can be solved analytically for any sets of boundary conditions in terms of the unknown constant N_x^0. After solving these equations, we will use one more condition to find the final solutions. In order to solve Eqs. (25) for convenience, the following state space variables are introduced:

$$\{X_1(x)\}=\{U(x)\},\qquad \{X_2(x)\}=\left\{\frac{dU}{dx}\right\}=\left\{\frac{dX_1}{dx}\right\},$$

$$X_3(x)=w(x),\qquad X_4(x)=\frac{dw}{dx}=\frac{dX_3}{dx}, \tag{27}$$

where $\{X_1\}^T=[U_1,U_2,\ldots,U_{N+1}]$ and $\{X_2\}^T=[dU_1/dx,dU_2/dx,\ldots,dU_{N+1}/dx]$.

Substitution of Eqs. (27) into Eqs. (25) results in a system of $2N+4$ coupled first-order ordinary differential equations which, on the other hand, may be presented as:

$$\left\{\frac{dX}{dx}\right\}=[A]\{X\}+\{F\}, \tag{28}$$

with $\{X\}^T=[\{X_1\}^T,\{X_2\}^T,X_3,X_4]$. In Eq. (28) the coefficient matrix $[A]$ and vector $\{F\}$ are presented in Appendix A. The general solutions of Eqs. (28) are given by (e.g. see Franklin, 1968):

$$\{X\}=[\mathbf{U}]\big[Q(\lambda x)\big]\{K\}+[\mathbf{U}]\big[Q(\lambda x)\big]\int\big[Q(\lambda x)\big]^{-1}[\mathbf{U}]^{-1}\{F\}\,dx, \tag{29}$$

with $[Q(\lambda x)]=\mathrm{diag}(e^{\lambda_1 x},e^{\lambda_2 x},\ldots,e^{\lambda_{2N+4}x})$ and $\{K\}$ being $2N+4$ arbitrary unknown constants of integration to be found by imposing the boundary conditions. Here, $[\mathbf{U}]$ and λ_k $(k=1,2,\ldots,2N+4)$ are, respectively, the matrix of eigenvectors and eigenvalues of the coefficient matrix $[A]$ which, in general, must be regarded to have complex values.

Next, in order to obtain N_x^0 we note that for the C1-C1 and S1-S1 boundary types we have $u_0=0$ at $x=\pm a/2$ which will allow us to find N_x^0 in a trial and error process. Towards this end, we note that integrating Eq. (23) from 0 to $a/2$ results in:

$$[u_0]\big|_{x=0}^{x=a/2}=\int_0^{a/2}\left[\frac{1}{A_{11}}\left(N_x^0+N_x^T-B_{11}^{j}\frac{dU_j}{dx}\right)-\frac{1}{2}\left(\frac{dw}{dx}\right)^2\right]dx. \tag{30}$$

Clearly, because of symmetry we have $u_0(0)=0$. Therefore, we conclude that:

$$N_x^0=\frac{2A_{11}}{a}\int_0^{a/2}\left[\frac{B_{11}^{j}}{A_{11}}\frac{dU_j}{dx}+\frac{1}{2}\left(\frac{dw}{dx}\right)^2\right]dx-N_x^T. \tag{31}$$

By making the solutions of Eqs. (29) to satisfy (31) in a trial and error process, we will obtain the exact value of N_x^0. Finally, u_0 will be found by integrating Eq. (23) as:

$$u_0=-\int\frac{1}{2}\left(\frac{dw}{dx}\right)^2dx+\frac{N_x^0+N_x^T}{A_{11}}x-\frac{B_{11}^{j}U_j}{A_{11}}. \tag{32}$$

3.2. Perturbation technique

In this section, a perturbation technique is used to solve the three coupled non-linear ordinary differential equations appearing in (9). To this end, we define W_0 as follows:

$$w(0)=W_0. \tag{33}$$

Also the unknown variables in Eqs. (1) are represented by the following expansions:

$$u_0(x)=u_1(x)W_0^1+u_2(x)W_0^2+u_3(x)W_0^3+\cdots, \tag{34a}$$

$$U_k(x)=U_k^1(x)W_0^1+U_k^2(x)W_0^2+U_k^3(x)W_0^3+\cdots,\quad k=1,2,\ldots,N+1, \tag{34b}$$

$$w(x)=w_1(x)W_0^1+w_2(x)W_0^2+w_3(x)W_0^3+\cdots, \tag{34c}$$

where W_0 is an unknown parameter which will be found at the end of analysis. Next, in the mechanical loading ($\Delta T=0$) we let:

$$q=q_1W_0^1+q_2W_0^2+q_3W_0^3+\cdots. \tag{35}$$

Also in thermal loading ($q(x)=0$) we consider the change of temperature of the top surface of the plate as ΔT. Using Eq. (17) the temperature field is known in terms of ΔT. Next, in this case, we let:

$$\Delta T=\Delta T_1W_0^1+\Delta T_2W_0^2+\Delta T_3W_0^3+\cdots, \tag{36}$$

where q_i's and ΔT_i's are some unknown constants which will be obtained by imposing certain conditions. These conditions are found by noting that from (33) and (34c) we must conclude that:

$$w_1(0)=1,$$

$$w_i(0)=0,\quad i=2,3,\ldots. \tag{37}$$

Substituting Eqs. (34) and (35) (or (36)) into Eqs. (12) and the subsequent results into Eqs. (9), yields infinite sets of coupled linear ordinary differential equations. For example, three first sets of equations for the mechanical loading case are:

W_0^1:

$$\begin{aligned}
&A_{11}\frac{d^2u_1}{dx^2}+B_{11}^{j}\frac{d^2U_j^1}{dx^2}=0,\\
&B_{11}^{k}\frac{d^2u_1}{dx^2}+D_{11}^{kj}\frac{d^2U_j^1}{dx^2}-A_{55}^{kj}U_j^1-A_{55}^{k}\frac{dw_1}{dx}=0,\\
&A_{55}\frac{d^2w_1}{dx^2}+A_{55}^{j}\frac{dU_j^1}{dx}=-q_1,
\end{aligned} \tag{38a}$$

W_0^2:

$$\begin{aligned}
&A_{11}\frac{d^2u_2}{dx^2}+B_{11}^{j}\frac{d^2U_j^2}{dx^2}=-A_{11}\frac{dw_1}{dx}\frac{d^2w_1}{dx^2},\\
&B_{11}^{k}\frac{d^2u_2}{dx^2}+D_{11}^{kj}\frac{d^2U_j^2}{dx^2}-A_{55}^{kj}U_j^2-A_{55}^{k}\frac{dw_2}{dx}=-B_{11}^{k}\frac{dw_1}{dx}\frac{d^2w_1}{dx^2},\\
&A_{55}\frac{d^2w_2}{dx^2}+A_{55}^{j}\frac{dU_j^2}{dx}=-q_2-A_{11}\frac{du_1}{dx}\frac{d^2w_2}{dx^2}\\
&\qquad\qquad -B_{11}^{j}\frac{dU_j^1}{dx}\frac{d^2w_1}{dx^2},
\end{aligned} \tag{38b}$$

W_0^3:

$$\begin{aligned}
&A_{11}\frac{d^2u_3}{dx^2}+B_{11}^{j}\frac{d^2U_j^3}{dx^2}=-A_{11}\left(\frac{dw_1}{dx}\frac{d^2w_2}{dx^2}+\frac{dw_2}{dx}\frac{d^2w_1}{dx^2}\right),\\
&B_{11}^{k}\frac{d^2u_3}{dx^2}+D_{11}^{kj}\frac{d^2U_j^3}{dx^2}-A_{55}^{kj}U_j^3-A_{55}^{k}\frac{dw_3}{dx}
\end{aligned}$$

$$= -B_{11}^{k}\left(\frac{dw_1}{dx}\frac{d^2w_2}{dx^2} + \frac{dw_2}{dx}\frac{d^2w_1}{dx^2}\right),$$

$$A_{55}\frac{d^2w_3}{dx^2} + A_{55}^{j}\frac{dU_j^3}{dx} = -q_3 - A_{11}\left[\frac{du_1}{dx}\frac{d^2w_2}{dx^2} + \frac{du_2}{dx}\frac{d^2w_1}{dx^2} + \frac{1}{2}\left(\frac{dw_1}{dx}\right)^2\frac{d^2w_2}{dx^2}\right] - B_{11}^{j}\left(\frac{dU_j^1}{dx}\frac{d^2w_2}{dx^2} + \frac{dU_j^2}{dx}\frac{d^2w_1}{dx^2}\right). \quad (38c)$$

After the solution for these sets of equations are obtained, then the constants q_i's (or ΔT_i's) are found by imposing the conditions in (37). Finally, W_0 is found by numerically solving the polynomial equation in (35) (or (36)).

For unsymmetric bending of the plate that is subjected to both mechanical and thermal loadings, we define the following parameters:

$$w(0) = W_0, \qquad u_0(0) = U_0. \quad (39)$$

Also the unknown variables in Eqs. (1) are represented by the following expansions:

$$u_0(x) = u_{10}(x)W_0^1 + u_{01}(x)U_0^1 + u_{11}(x)W_0^1U_0^1 + u_{20}(x)W_0^2 + u_{02}(x)U_0^2 + u_{21}(x)W_0^2U_0^1 + u_{12}(x)W_0^1U_0^2 + \cdots, \quad (40a)$$

$$U_k(x) = U_k^{10}(x)W_0^1 + U_k^{01}(x)U_0^1 + U_k^{11}(x)W_0^1U_0^1 + U_k^{20}(x)W_0^2 + U_k^{02}(x)U_0^2 + U_k^{21}(x)W_0^2U_0^1 + U_k^{12}(x)W_0^1U_0^2 + \cdots, \quad k = 1, 2, \ldots, N+1, \quad (40b)$$

$$w(x) = w_{10}(x)W_0^1 + w_{01}(x)U_0^1 + w_{11}(x)W_0^1U_0^1 + w_{20}(x)W_0^2 + w_{02}(x)U_0^2 + w_{21}(x)W_0^2U_0^1 + w_{12}(x)W_0^1U_0^2 + \cdots. \quad (40c)$$

Furthermore, we let:

$$q = q_{10}(x)W_0^1 + q_{01}(x)U_0^1 + q_{11}(x)W_0^1U_0^1 + q_{20}(x)W_0^2 + q_{02}(x)U_0^2 + q_{21}(x)W_0^2U_0^1 + q_{12}(x)W_0^1U_0^2 + \cdots,$$

$$\Delta T = \Delta T_{10}(x)W_0^1 + \Delta T_{01}(x)U_0^1 + \Delta T_{11}(x)W_0^1U_0^1 + \Delta T_{20}(x)W_0^2 + \Delta T_{02}(x)U_0^2 + \Delta T_{21}(x)W_0^2U_0^1 + \Delta T_{12}(x)W_0^1U_0^2 + \cdots, \quad (41)$$

where q_{ij}'s and ΔT_{ij}'s are some unknown constants which will be obtained by imposing certain conditions. These conditions are found by noting that from (39), (40a), and (40c) we must conclude that:

$$w_{10}(0) = 0, \quad w_{01}(0) = w_{11}(0) = w_{20}(0) = \cdots = 0,$$
$$u_{10}(0) = 0, \quad u_{01}(0) = u_{11}(0) = u_{20}(0) = \cdots = 0. \quad (42)$$

Substituting Eqs. (40) and (41) into Eqs. (12) and the subsequent results into Eqs. (9), yields infinite sets of coupled linear ordinary differential equations. By using (42) q_{ij}'s and ΔT_{ij}'s are found. Finally, W_0 and U_0 are obtained by numerically solving the polynomial equation in (41).

4. Numerical results and discussion

The solution procedures outlined in the previous section are applied to functionally graded plates subjected to a uniform distributed load and/or a steady state thermal load. The total thickness of the plate is denoted by h with its side length being a. The side-to-thickness ratio (i.e., a/h) is assumed, unless otherwise mentioned, to be 15 in all numerical examples. Also the total thickness of the plate (h) is considered to be 0.01 m. It is assumed that the bottom surface of the plate is rich of metal (Aluminum) and the top surface is rich of ceramic (Zirconia). The thermomechanical properties of Aluminum and Zirconia are as follows (Reddy, 2000):

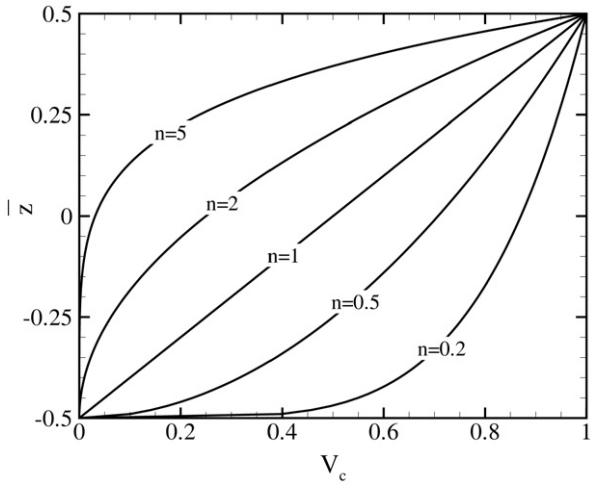

Fig. 1. Variation of the volume fraction of the ceramic phase through the thickness of the FGM plate.

$$E_m = 70 \text{ GPa}, \quad \nu_m = 0.3, \quad \alpha_m = 23 \times 10^{-6}/^\circ\text{C}, \quad k_m = 204 \text{ W/mK},$$
$$E_c = 151 \text{ GPa}, \quad \nu_c = 0.3, \quad \alpha_c = 10 \times 10^{-6}/^\circ\text{C}, \quad k_c = 2.09 \text{ W/mK}. \quad (43)$$

Fig. 1 shows the distribution of the volume fraction of the ceramic phase through the plate thickness for various values of the power-law index n. Note that the thickness coordinate has been non-dimensionalized.

In all numerical results, the linear Lagrangian interpolation function through the thickness is used. Also the total thickness of the FGM plate is divided into twenty numerical layers.

4.1. Mechanical loading

To study the non-linear bending behavior of functionally graded plates, some representative numerical results are presented for the plates subjected to a uniform transverse load. In the numerical results the various non-dimensional parameters used are:

$$\text{side coordinate } \bar{x} = x/a,$$
$$\text{thickness coordinate } \bar{z} = z/h,$$
$$\text{deflection } \bar{w} = w/h,$$
$$\text{axial stress } \bar{\sigma}_x = \sigma_x h^2/(q_0 a^2),$$
$$\text{load parameter } \bar{q} = q_0 a^4/(E_m h^4). \quad (44)$$

Here, q_0 denotes the intensity of the applied uniform transverse load. When both edges of the plate have S3 or C3 supports, it can be shown that the non-linear and linear results are identical. Here, for brevity, we will only present the numerical results, unless otherwise mentioned, for C1-C1 supports.

Fig. 2 presents the variation of the center deflection of the FGM plate with, for example, $n = 2$ versus the load parameter $\bar{q}$. It is seen that for the maximum deflections greater than $0.3h$ a non-linear solution is required. To check the correctness and accuracy of the present methods, the results achieved from these methods are compared with those obtained by utilizing the commercial finite element package of ANSYS. It is to be noted that the plate has

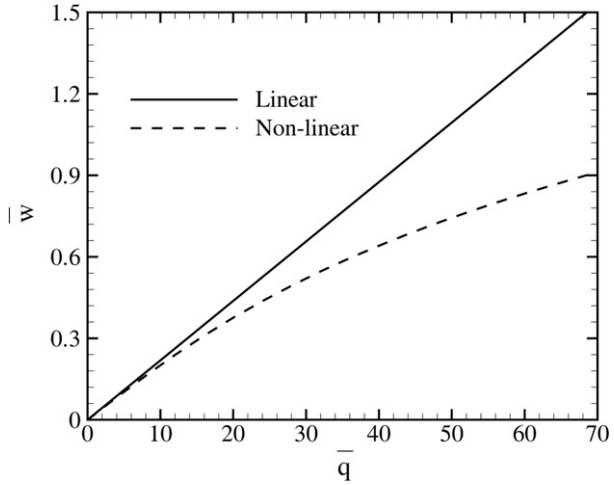

Fig. 2. Variation of the non-dimensional center deflection $\bar{w}$ of the FGM plate with $n = 2$ versus $\bar{q}$.

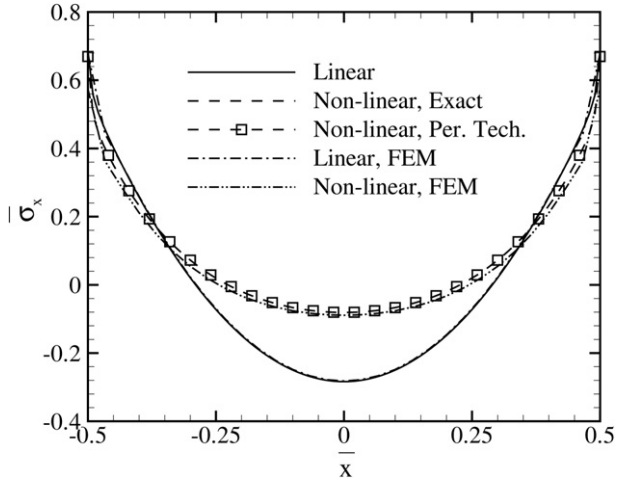

Fig. 3. Variation of the non-dimensional axial stress $\bar{\sigma}_x$ along the top surface of the FGM plate with $n = 2$ subjected to $\bar{q} = -70$.

Table 1
Comparisons of the results obtained in the present paper to the results obtained by FEM for the maximum non-dimensional deflection $\bar{w}$ of FGM plate with different material constant n and different boundary conditions under uniformly distributed transverse mechanical loading

Boundary conditions, Load	Material composition	FEM		Present	
		Linear	Non-linear	Linear	Non-linear
C1-C1, $\bar{q} = -70$	ceramic	0.994	0.724	0.979	0.711
	$n = 0.2$	1.207	0.829	1.101	0.760
	$n = 0.5$	1.365	0.889	1.245	0.810
	$n = 1$	1.501	0.935	1.396	0.860
	$n = 2$	1.645	0.996	1.532	0.911
	metal	2.145	1.128	2.111	1.117
S1-S1, $\bar{q} = -20$	ceramic	1.459	1.323	1.437	1.301
	$n = 0.2$	1.648	1.469	1.549	1.374
	$n = 0.5$	1.865	1.631	1.768	1.538
	$n = 1$	2.091	1.790	1.972	1.701
	$n = 2$	2.285	1.917	2.164	1.817
	metal	3.147	2.328	3.097	2.291

been modeled in ANSYS by using three-dimensional eight-noded structural solid elements and the total thickness of the plate has been subdivided into twelve layers. Comparisons of the results obtained in the present paper to the results obtained by finite element method (FEM) are shown in Table 1 for the maximum non-dimensional deflection $\bar{w}$ of FGM plate with different material constant n and two different boundary conditions (i.e., C1-C1 and S1-S1) under uniformly distributed transverse mechanical loading. Good agreements can be seen from Table 1, and the validity of the present methods is verified. It is to be noted that the numerical results showed that the two different solution methods presented in this paper result in identical transverse deflection.

Fig. 3 illustrate the variation of non-dimensional axial stress $\bar{\sigma}_x$ along the top surface of the plate, when $\bar{q} = -70$. It is seen from this figure that there is an excellent agreement between the present solutions and those of FEM. Also it is observed that the exact method and perturbation technique yield identical results. The numerical results in the perturbation technique showed that the numerical values of displacements and stresses are converged by using three first sets of equations as given by Eqs. (38). Hence, in the remainder of the present study only three sets of equations are used in the perturbation technique.

Fig. 4 illustrates the variation of the non-dimensional center deflection of the FGM plate with different values of the power-law index n subjected to a uniform transverse load. Also variation of the non-dimensional center deflection $\bar{w}$ of the FGM plate subjected to $q = 1 \times 10^6$ N/m^2 versus side-to-thickness ratio a/h for various values of the power-law index n are displayed in Fig. 5. The results show that a pure metal plate has highest deflection. This is expected because the fully metal plate is the one with the lower stiffness than the ceramic and FGM plates.

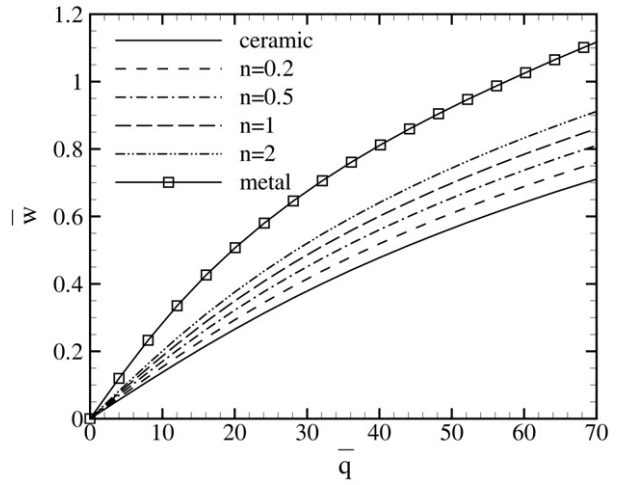

Fig. 4. Variation of the non-dimensional center deflection $\bar{w}$ of the FGM plate versus $\bar{q}$.

Figs. 6 and 7 show through the thickness distributions of the non-dimensional axial stress $\bar{\sigma}_x$ of the FGM plate subjected to $\bar{q} = -70$ for various values of the power-law index n in linear and non-linear analyses, respectively. Under the application of the pressure loading, the stresses are compressive at the top surface and tensile at the bottom surface. For the different power-law indices chosen, the plate corresponding to $n = 2$ in the linear analysis yielded the maximum compressive stress at the top surface. This is the ceramic rich surface.

4.2. Thermal loading

Here we present some numerical results for a representative simply supported plate (S1-S1) which is subjected to a thermal loading through its thickness direction. The temperature of the bottom metal-rich surface is kept constant at $T_m = 20\,^\circ$C and that of the top ceramic-rich surface is varied form $T_c = 20\,^\circ$C to $T_c = 300\,^\circ$C. A stress free temperature $T_0 = 20\,^\circ$C is assumed. The temperature field through the thickness of the plate can be easily obtained from Eq. (17).

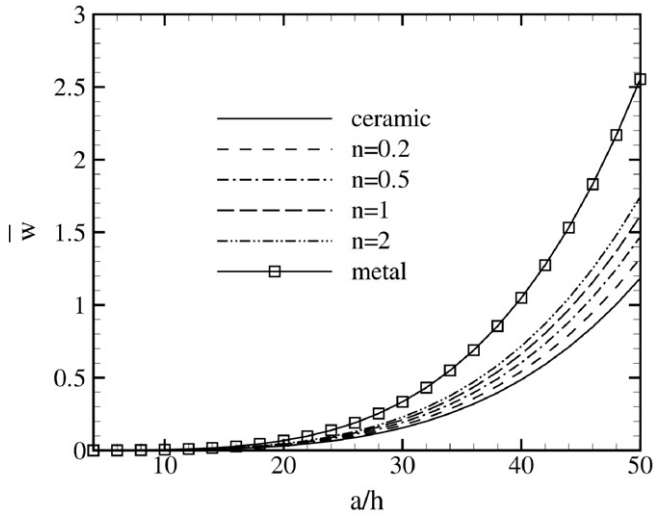

Fig. 5. Variation of the non-dimensional center deflection $\bar{w}$ of the FGM plate versus side-to-thickness ratio a/h.

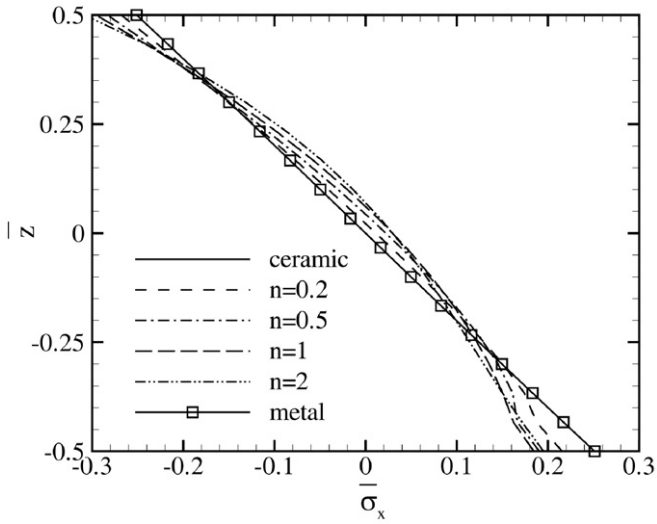

Fig. 6. Through the thickness distribution of non-dimensional axial stress $\bar{\sigma}_x$ of the FGM plate subjected to $\bar{q} = -70$ in linear analysis.

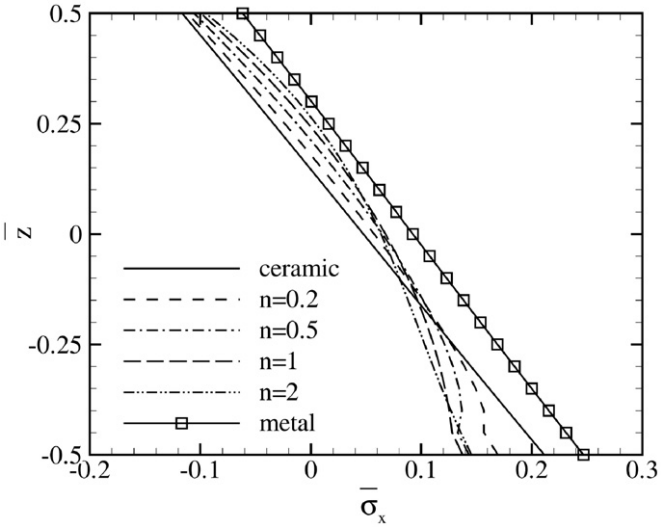

Fig. 7. Through the thickness distribution of non-dimensional axial stress $\bar{\sigma}_x$ of the FGM plate subjected to $\bar{q} = -70$ in non-linear analysis.

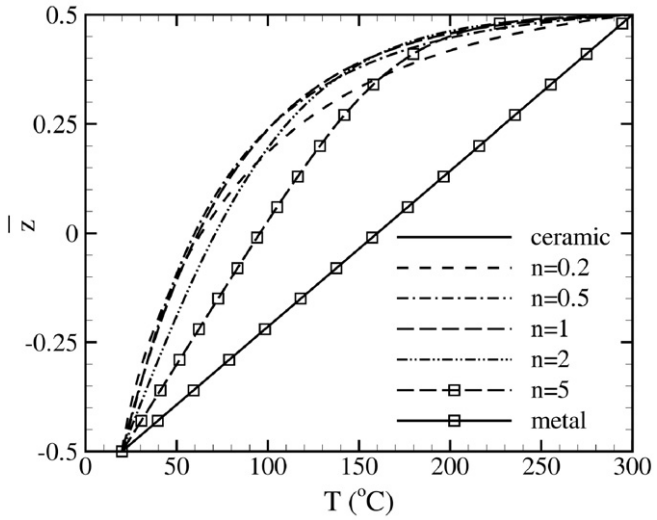

Fig. 8. Temperature profile through the thickness of the FGM plate.

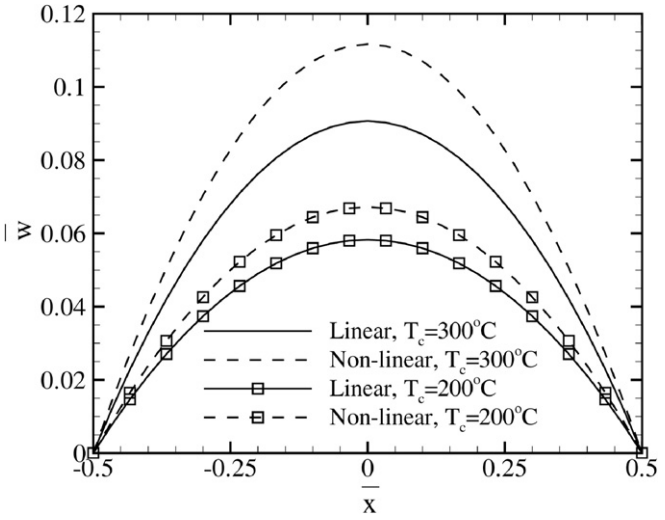

Fig. 9. Variation of the non-dimensional deflection $\bar{w}$ along the side of the FGM plate with $n = 2$.

Fig. 8 shows the variation of the temperature through the thickness of the FGM plate for various values of the power-law index n. It is seen that the temperature in the plates with both ceramic and metal is always greater than that corresponding to a fully ceramic or fully metallic plate.

The variation of non-dimensional deflection $\bar{w}$ along the side of the FGM plate with $n = 2$ when $T_c = 200\,^{\circ}\mathrm{C}$ and $T_c = 300\,^{\circ}\mathrm{C}$ is shown in Fig. 9. The deflection of the plate under the thermal loading is positive because the thermal expansion $\alpha\Delta T$ at the top surface is higher than that experienced by the bottom surface, and this expansion results in an upward deflection of the plate. The results of the linear analysis are also presented in the figure to highlight the difference between linear and non-linear responses with increasing the temperature of ceramic-rich surface. From the figure it can be observed that at higher temperature non-linear effects are predominant and deflection values are greater than the linear ones owing to the decreased structure stiffness due to contribution from the non-linear terms in the strain field.

Figs. 10 and 11 show, respectively, the linear and non-linear variations of the non-dimensional center deflection $\bar{w}$ with increasing the temperature of the top surface for the FGM and fully metallic and ceramic plates. By comparing Fig. 10 with Fig. 11, it is observed that the effect of non-linearity increased the cen-

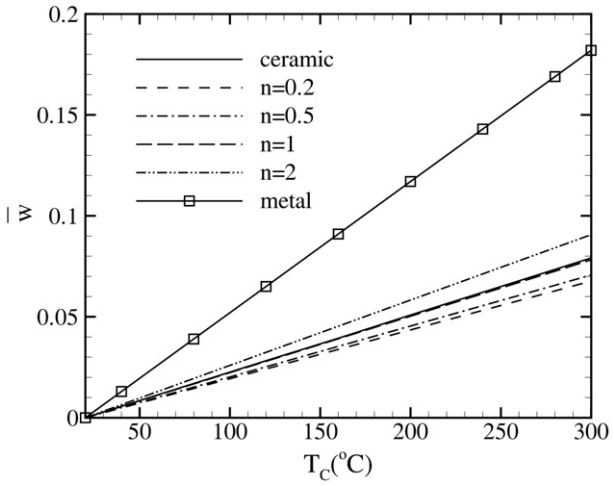

Fig. 10. Linear variation of the non-dimensional center deflection $\bar{w}$ with increasing the temperature of the top surface of the FGM plate.

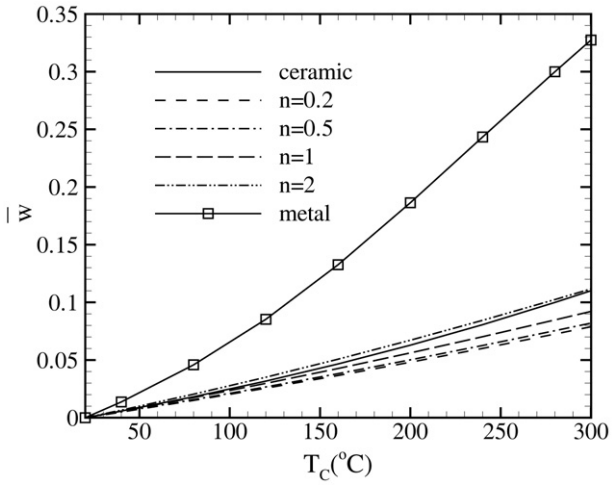

Fig. 11. Non-linear variation of the non-dimensional center deflection $\bar{w}$ with increasing the temperature of the top surface of the FGM plate.

ter deflection of the plates. Also it is seen form these figures that the fully metal plate has greater center deflection in compared to FGM and fully ceramic plates. It is to be noted that the deflection depends on the product of the temperature and the thermal expansion coefficient. Therefore, the response of the graded plates is not intermediate to the metal and ceramic plates. The deflection of the FGM plate corresponding to $n = 0.2$ seems to be a minimum. Note that the temperature profiles for the various plates are close to each other, and this probably is the reason why the deflections under temperature field for the various graded plates are also close to each other.

The variation of the non-dimensional deflection $\bar{w}$ along the side of the clamped-simply supported (C1-S1) FGM plate with $n = 2$ when $T_c = 200\,^{\circ}\mathrm{C}$ and $T_c = 300\,^{\circ}\mathrm{C}$ is shown in Fig. 12. It is seen that the non-linearity effect is also significant in this kind of boundary condition.

4.3. Thermomechanical loading

In this section, it is assumed that the FGM plate is subjected to non-dimensional uniform transverse load $\bar{q} = 1$ in the presence of the temperature field through the thickness of the plate. The temperature of the bottom and top surfaces are kept constant at $T_m = 20\,^{\circ}\mathrm{C}$ and $T_c = 200\,^{\circ}\mathrm{C}$, respectively. Also the side-to-thickness

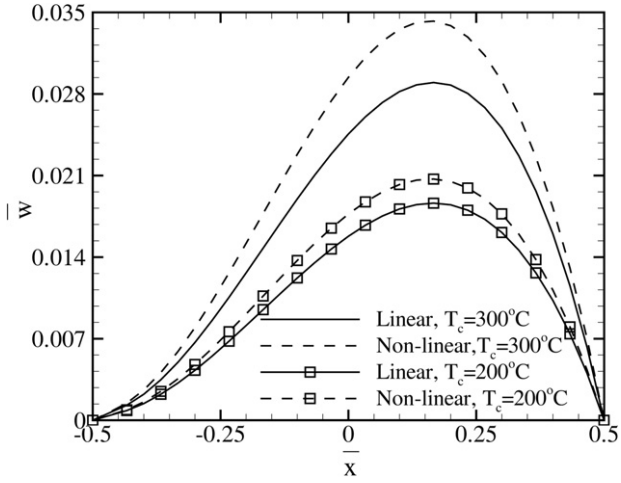

Fig. 12. Variation of the non-dimensional deflection $\bar{w}$ along the side of the C1-S1 FGM plate with $n = 2$.

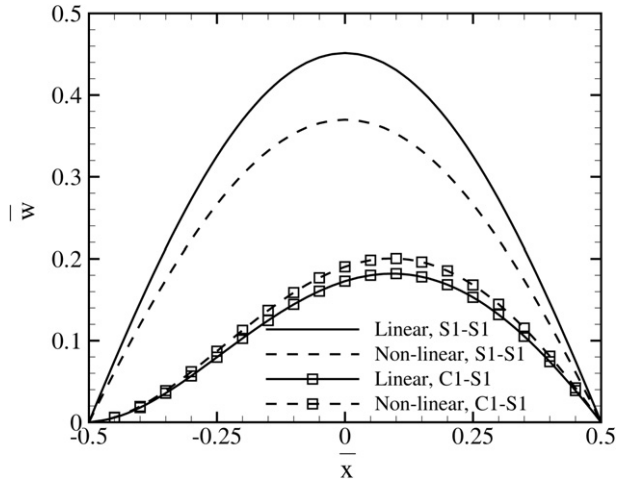

Fig. 13. Variation of the non-dimensional deflection $\bar{w}$ along the side of the S1-S1 and C1-S1 FGM plates with $n = 2$.

ratio of the FGM plate is assumed to be 20 in all numerical examples.

Fig. 13 illustrate the variation of the non-dimensional deflection $\bar{w}$ along the side of the FGM plate with $n = 2$ and two different boundary conditions S1-S1 and C1-S1. The deflection of the plates under thermomechanical loading is positive because the thermal expansion at the top surface is higher due to the higher thermal expansion, and this expansion results in an upward deflection of the plate. Moreover, a positive (upward) transverse load is applied to the plates. It is observed that in this kind of thermomechanical loading, the effect of non-linearity is to lower the magnitude of the transverse deflection for S1-S1 boundary conditions and is to higher for C1-S1 boundary conditions.

Finally, the variation of the non-dimensional axial stress $\bar{\sigma}_x$ along the top surface of the FGM plate with $n = 2$ is displayed in Fig. 14.

5. Conclusions

In this study, based on a layerwise theory, FGM plates in cylindrical bending subjected to distributed transverse mechanical, thermal and combined thermomechanical loadings are analyzed. Material properties are assumed to be graded in the thickness direction according to a simple power-law distribution in terms of the volume fractions of the constituents. The non-linear strain–

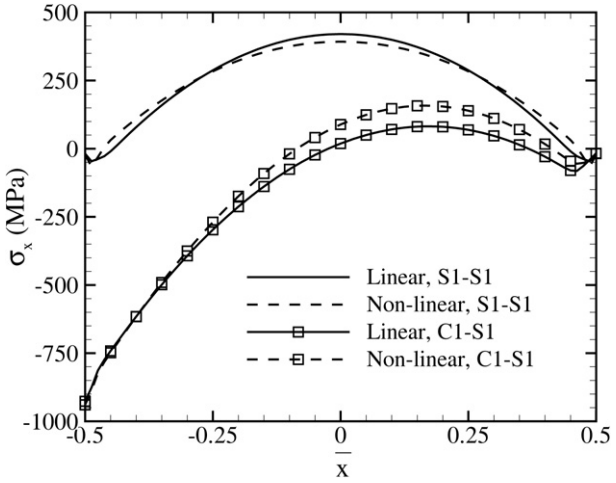

Fig. 14. Variation of the non-dimensional axial stress $\bar{\sigma}_x$ along the top surface of the S1-S1 and C1-S1 FGM plates with $n = 2$.

displacement relations of the von Kármán-type are used to study the effect of geometric non-linearity. The equilibrium equations are solved exactly and also by using a perturbation technique. The results obtained from these methods are presented for various loading and boundary conditions. Also non-dimensional stresses and deflection are computed for plates with two different ceramic-metal mixtures. The numerical results show that the non-linearity effect on the plate responses is significant. On the other hand, the results indicate that the effect of non-linearity is to lower the magnitude of the transverse deflection in mechanical loading and is to higher in thermal loading. Finally, it is shown that in thermal loading case deflection in the center of fully metal plate is higher than that of fully ceramic and FGM plates.

Acknowledgement

The authors would like to thank the Khorasan Research Center for Technology Development (KRCTD) supporting this work.

Appendix A

The coefficient matrix $[A]$ and vector $\{F\}$ appearing in Eqs. (28) are defined as:

$$[A] = \begin{bmatrix} [0] & [I] & \{0\} & \{0\} \\ [a_1] & [0] & \{0\} & [a_2] \\ \{0\}^T & \{0\}^T & 0 & 1 \\ \{0\}^T & \{b_1\}^T & b_2 & 0 \end{bmatrix}, \qquad \{F\} = \begin{Bmatrix} \{0\} \\ \{0\} \\ 0 \\ f \end{Bmatrix},$$

where [0] and $[I]$ are $(2N+4)\times(2N+4)$ square and zero identity matrices, respectively, and $\{0\}$ is a zero vector with $2N+4$ rows. The remaining matrices and constants in the above equations are:

$$[a_1] = \left([D_{11}] - \{B_{11}\}\{B_{11}\}^T/A_{11}\right)^{-1}\left([A_{55}] + [\varepsilon]\right),$$

$$[a_2] = \left([D_{11}] - \{B_{11}\}\{B_{11}\}^T/A_{11}\right)^{-1}\{A_{55}\},$$

$$\{b_1\} = -\{A_{55}\}/\left(A_{55} + N_x^0\right),$$

$$b_2 = \varepsilon/\left(A_{55} + N_x^0\right),$$

$$f = -q_0/\left(A_{55} + N_x^0\right).$$

References

Agarwal, S., Chakraborty, A., Gopalakrishnan, S., 2006. Large deformation analysis for anisotropic and inhomogeneous beams using exact linear static solutions. Compos. Struct. 72, 91–104.

Franklin, J.N., 1968. Matrix Theory. Prentice-Hall, Englewood Cliffs, NJ.

Fung, Y.C., 1965. Foundation of Solid Mechanics. Prentice-Hall, Englewood Cliffs, NJ.

Hsieh, J.-J., Lee, L.-T., 2006. An inverse problem for a functionally graded elliptical plate with large deflection and slightly disturbed boundary. Int. J. Solids Struct. 43 (20), 5981–5993.

Noda, N., Tsuji, T., 1991. Steady thermal stresses in a plate of functionally gradient material. Trans. Japan Soc. Mech. Engineers, Ser. A 57, 98–103.

Nosier, A., Kapania, R.K., Reddy, J.N., 1993. Free vibration analysis of laminated plates using a layerwise theory. AIAA J. 31 (12), 2335–2346.

Praveen, G.N., Reddy, J.N., 1998. Nonlinear transient thermoelastic analysis of functionally graded ceramic-metal plates. Int. J. Solids Struct. 35 (33), 4457–4476.

Reddy, J.N., 1987. A generalization of two-dimensional theories of laminated composite plates. Commun. Appl. Numer. Methods 3, 173–180.

Reddy, J.N., 2000. Analysis of functionally graded plates. Int. J. Numer. Meth. Engrg. 47, 663–684.

Reddy, J.N., Cheng, Z.Q., 2001. Three-dimensional thermo-mechanical deformations of functionally graded rectangular plates. Eur. J. Mech. A/Solids 20, 841–855.

Reddy, J.N., Chin, C.D., 1998. Thermoelastical analysis of functionally graded cylinders and plates. J. Thermal Stresses 21, 593–626.

Shen, H.-S., 2002. Nonlinear bending response of functionally graded plates subjected to transverse loads and in thermal environments. Int. J. Mech. Sci. 44, 561–584.

Tahani, M., Nosier, A., 2003. Free edge stress analysis of general cross-ply composite laminates under extension and thermal loading. Compos. Struct. 60, 91–103.

Tahani, M., Nosier, A., 2004. Accurate determination of interlaminar stresses in general cross-ply laminates. Mech. Adv. Mater. Struct. 11 (1), 67–92.

Tahani, M., Torabizadeh, M.A., Fereidoon, A., 2006. Nonlinear analysis of functionally graded beams. J. Achievements in Mater. Manufacturing Engrg. 18 (1–2), 315–318.

Tanigawa, Y., Akai, T., Kawamura, R., Oka, N., 1996. Transient heat conduction and thermal stress problems of a nonhomogeneous plate with temperature-dependent material properties. J. Thermal Stresses 19, 77–102.

Woo, J., Meguid, S.A., 2001. Nonlinear analysis of functionally graded plates and shallow shells. Int. J. Solids Struct. 38, 7409–7421.

Yang, J., Shen, H.-S., 2003. Non-linear analysis of functionally graded plates under transverse and in-plane loads. Int. J. Non-Linear Mech. 38, 467–482.